IEEE Access
Multidisciplinary | Rapid Review | Open Access Journal

Received 10 June 2023, accepted 4 July 2023, date of publication 10 July 2023, date of current version 20 July 2023.

Digital Object Identifier 10.1109/ACCESS.2023.3294109

RESEARCH ARTICLE

Design of an Optimal Control Strategy for Coupled Tank Systems Using Nonlinear Constraint Optimization With Kharitonov-Hurwitz Stability Analysis

K. R. ACHU GOVIND[1], SUBHASISH MAHAPATRA[1], (Senior Member, IEEE), AND SOUMYA RANJAN MAHAPATRO[2], (Member, IEEE)

[1]School of Electronics Engineering, VIT-AP University, Amaravati, Andhra Pradesh 522237, India
[2]School of Electronics Engineering, Vellore Institute of Technology, Chennai, Tamil Nadu 600127, India

Corresponding author: Subhasish Mahapatra (subhasish110@gmail.com; subhasish.m@vitap.ac.in)

This work was supported by the Vellore Institute of Technology Andhra Pradesh (VIT-AP) University.

ABSTRACT The fundamentals of nonlinear constraint optimization are exploited in this paper to design a decentralized PID controller for variable area coupled tank systems. Maintaining the tanks at the desired level is the main objective of the proposed decentralized control algorithm. The benchmark coupled tank systems are modeled to the first order plus dead time (FOPDT) model by designing decoupled subsystems. The control law is designed for decoupled systems to attain the servo response by minimizing loop interactions. Further, the overshoot is reduced by imposing constraints on the maximum closed-loop amplitude ratio of the system. Furthermore, the robustness of the controller is analyzed and stability is verified with the Kharitonov-Hurwitz theorem. A concise comparison is carried out between the proposed control law with existing methods in order to highlight the productive application of the proposed control algorithm. From the results, it envisaged that the proposed controller shows better responses compared to the existing methods. Besides, the efficacious nature of the proposed control scheme is validated by considering a wide range of closed-loop amplitude ratios.

INDEX TERMS Coupled tank systems, decouplers, FOPDT model, model uncertainty, PID control, stability analysis.

I. INTRODUCTION

Automatic liquid level regulation is essential in process control industries. An interacting tank system is a nonlinear multi-input multi-output (MIMO) system. Hence, regulating the level is a difficult task. Cross couplings and interaction between the variables are phenomenal characteristics of the MIMO systems. In addition, the closed-loop performance will be affected by time delays and parameter uncertainties. Hence, compared to single-loop systems, regulating the necessary parameters with interactions is very difficult. The following literature describes different control techniques for coupled tank systems.

Article [1] exploits the stability analysis of the quadruple tank system (QTS). Further, the PI controller is designed to achieve the design specifications. A hybrid controller (combination of state feedback and sliding mode controller) for the QTS is presented in [2]. The steady-state error is reduced by the state feedback controller while the sliding mode controller guarantees a transient response. The design specifications of the QTS can be achieved with the sliding mode controller as reported in [3]. Albeit, the servo response can be achieved, the system fails to attain regulatory response. As discussed in [4], the servo response is ensured with a PI controller. The controller parameters

The associate editor coordinating the review of this manuscript and approving it for publication was Laura Celentano.

for the QTS are derived from bond-graph prototyping. The design specifications of the QTS are attained with a linear quadratic Gaussian regulator as described in [5] The control law is realized with a model predictive technique. Article [6] reports a fuzzy controller for maintaining the level of a conical tank system (CTS). Besides, Kalmann algorithm was used to define the fuzzy rules. Further, the desired servo response was attained by adjusting the controller parameters with the defined algorithm. As described in [7], a fractional order passivity-based control law is implemented for the CTS. The overshoot is reduced and the design criteria are attained. The level of the CTS is regulated with a smart controller as discussed in [8]. The control law is based on a reinforcement learning algorithm. Further, the system is represented by the Markov decision process and the Q-learning algorithm is used to realize the control law. A fractional-order-proportional-integral-derivative controller (FOPID) for the CTS is addressed in [9]. A fault tolerant control system for an interacting CTS is exploited in [10]. The controller gains were obtained from the Takagi-Sugeno (T-S) fuzzy model. Further, a cost function was defined to minimize the error. Furthermore, the particle swarm optimization techniques were used to determine the FOPID controller parameters. Various optimization methods are presented in [11] for controlling the level of the CTS. However, it was inferred that the bubble-net whale optimization algorithm can satisfy design requirements. The desired level can be attained in a spherical tank system (STS) with a sliding mode controller as described in [12]. As discussed in [13], the level of STS was maintained with a PI controller. The control parameters were obtained from the root locus method and the design criteria are satisfied. Articles [14], [15], [16], [17], and [18] report different control strategies for controlling the level of STS. A PI controller tuned with the genetic algorithm is addressed in [19] for maintaining the level of STS. From the aforementioned literature, it can be inferred that in a centralized control structure, the system performance is affected by loop interactions. Albeit the interactions can be reduced with the off-diagonal controller or full controller structure, the design procedure is complicated since the tuning need to be performed individually for loop controllers. On the other hand, decentralized controllers have a simple structure as the tuning needs to be performed only for diagonal elements. The recent advancements in decentralized control schemes are given below.

Various model predictive control schemes for the QTS are presented in [20]. However, it was inferred that the desired servo and regulatory response was achieved with the multi-parametric model decentralized PI controller. In [21], a relay-based control law for the QTS is reported. The PID controller gains are obtained from the relay-based tuning method. Sliding mode controllers were designed to attain the design criteria for the QTS as discussed in [22] and [23]. Albeit, the servo response is achieved, the robustness of the system is not verified. A nonlinear disturbance-observer for the QTS is presented in [24] wherein the coupling characteristics are used to design the controller. Further, the Lyapunov theorem was used to verify the stability of the system. A decentralized control technique for the CTS is addressed in [25]. The servo response was attained with the decentralized PI controller. Further, a multi-variable Nyquist plot was used to analyze the stability of the system. A dynamic matrix controller that ensures the design specifications of a CTS is exploited in [26]. A fractional-order controller for the interacting CTS is presented in [27]. The control structure is implemented with simplified decouplers and an equivalent-transfer function model. Besides, the PID control parameters were derived from the bat optimization algorithm. Article [28] reports a fuzzy-fractional-order PI controller for the coupled CTS. The controller gains are derived from the metaheuristic algorithm. Further, the Lyapunov theorem is used to analyze the stability. A gain scheduled PI controller is discussed in [29] for maintaining the level of the STS. As described in [30], a comparative analysis based on the Performance Indexes was made with different controllers for an interacting spherical tank system. However, it was inferred that with fractional order fuzzy PID controllers, the design specifications can be attained. A fuzzy PI controller for STS is addressed in [31]. The decouplers were designed with an inverted decoupling structure. The level of the coupled STS is maintained with a multi-model-cascade-control structure as exploited in [32]. A decentralized PID controller for interacting tank systems is presented in [33]. The controller is designed based on the frequency domain specifications. Articles [34] and [35] reports various optimization-based techniques for attaining the design specifications. An adaptive controller based on the neural network to stabilize the maglev vehicle is discussed in [36]. The stability of the system is analyzed with Lyapunov stability theorem. The sensor error compensation of a magneto-resistive material employing geometry-constraint-contour scaling is described in [37]. Besides, the article provides a description about various parameter estimation methods. A closed-loop parameter identification algorithm for second-order nonlinear systems is addressed in [38]. The algorithm employs least squares and state estimation to estimate the system parameters. Besides, the robustness is verified with Monte-Carlo analysis.

Thus, from the aforementioned literature, it is very clear that albeit the servo response is attained with various controllers, there exists a trade-off between the performance of the controller and robustness. The design specifications are attained with the reported controllers however, the stability needs to be compromised. Thus, the main objective of the work is to design a decentralized control algorithm based on nonlinear constraint optimization. The crucial performance criteria can be achieved from the parameters like bandwidth and closed-loop amplitude ratio (AR). The settling time can be considerably reduced with a higher value of bandwidth. Similarly, a faster response can be obtained with a high value

for AR. However, the performance of the system will be degraded. Hence to achieve the desired closed-loop performance, the values of bandwidth and AR must be properly chosen. Further, by imposing constraints on AR, the overshoot can be reduced. Furthermore, robustness can be ensured by considering the frequency domain specifications. The robustness of the controller is analyzed with input, output noise signals and a range of parameter uncertainties. Besides, the stability is analyzed with the Kharitonov theorem. The controller performance is verified for interacting coupled tank systems. Thus, the main contributions of this paper can be summarized as

- Design of decentralized PID controller to attain the design requirements of the coupled tank systems.
- The regulatory response is analyzed with input and output disturbances.
- The robustness analysis of the system is verified by considering input and output uncertainties.
- Analyze the response of the controller to parameter uncertainties.
- Analysis of the robust stability is carried out by the Kharitonov-Hurwitz theorem.

The remaining paper is organized as follows: Section II describes the problem statement. The decoupler design is explained in Section II-A. The necessary steps for the controller design is given in Section III. The Stability and Robustness property of the controller is discussed in Section IV. Simulation results are presented in Section V followed by conclusion in Section VI.

II. DESCRIPTION OF PROBLEM

The modeling of decouplers for the two input two output (TITO) system is described in this section. The TITO system $\mathcal{P}(s)$ can be represented as Equation (1)

$$\mathcal{P}(s) = \begin{bmatrix} p_{11}(s)e^{-\mu_{11}s} & p_{12}(s)e^{-\mu_{12}s} \\ p_{21}(s)e^{-\mu_{21}s} & p_{22}(s)e^{-\mu_{22}s} \end{bmatrix} \tag{1}$$

where the plant parameters are given by $p_{11}(s)e^{-\mu_{11}s}$, $p_{12}(s)e^{-\mu_{12}s}$, $p_{21}(s)e^{-\mu_{21}s}$, $p_{22}(s)e^{-\mu_{22}}s$ and μ_{ii} is the delay. Designing decouplers will decrease the loop interactions. Decoupler input is the output of controller, while the process input is the output of decoupler. Further, the control scheme is implemented to attain the design specifications.

A. DECOUPLER DESIGN

This subsection describes the decoupler design technique. The inverted decoupling method is described in [41] and [42]. Figure 1 presents the schematic of the TITO system. Further, for the TITO system, the decoupler matrix $\mathcal{D}(s)$ is defined by

$$\mathcal{D}(s) = \begin{bmatrix} 0 & -\frac{p_{12}(s)}{p_{11}(s)} \\ -\frac{p_{21}(s)}{p_{22}(s)} & 0 \end{bmatrix} \tag{2}$$

The process transfer matrix $\mathcal{Z}(s)$ is

$$\mathcal{Z}(s) = \mathcal{P}(s) * \mathcal{D}(s) = diag\{z_{11}(s), z_{22}(s)\} \tag{3}$$

The decoupled elements z_{ii} $(i = 1, 2)$ needs to be controlled by the proposed controller.

B. MODEL REDUCTION

Designing of the decoupled controller is difficult because of the complex dynamics of Equation (3). Besides, model reduction techniques are essential in addressing computational challenges, facilitating system understanding and design, enabling efficient control and optimization, and improving uncertainty analysis. By simplifying complex models while retaining essential dynamics, model reduction helps to overcome practical limitations and gain valuable insights. Hence suitable model reduction techniques are used to derive the FOPDT model structure as reported in [54] and [56]. The process dynamics $\mathcal{G}_{ii}(s)$ are given by

$$\mathcal{G}_{ii}(s) = \frac{\mathcal{K}_{ii}e^{-\Phi_{ii}s}}{\mathcal{T}_{ii}s + 1}, j = 1, 2 \tag{4}$$

where, $\mathcal{K}_{ii}$ is the process gain, Φ_{ii} is the time constant, and $\mathcal{T}_{ii}$ is the effective dead time. Further, to determine the unknown parameters, frequency response fitting is obtained at two points $\omega = 0$ and $\omega = \omega_{\mathcal{C}ii}$, where $\omega_{\mathcal{C}ii}$ is phase crossover frequency.

$$\mathcal{G}_{ii}(0) = \mathcal{Z}_{ii}(0) \tag{5}$$

$$|\mathcal{G}_{ii}(j\omega_{\mathcal{C}ii})| = |\mathcal{Z}_{ii}(j\omega_{\mathcal{C}ii})| \tag{6}$$

$$\angle\{\mathcal{G}_{ii}(j\omega_{\mathcal{C}ii})\} = \angle\{\mathcal{Z}_{ii}(j\omega_{\mathcal{C}ii})\} \tag{7}$$

The FOPDT parameters described in Equation (4) are determined as

$$\mathcal{K}_{ii} = \mathcal{Z}_{ii}(0) \tag{8}$$

$$\mathcal{T}_{ii} = \sqrt{\frac{\mathcal{K}_{ii}^2 - |\mathcal{Z}_{ii}(j\omega_{\mathcal{C}ii})|^2}{|\mathcal{Z}_{ii}(j\omega_{\mathcal{C}ii})|^2\omega_{\mathcal{C}ii}^2}} \tag{9}$$

$$\Phi_{ii} = \frac{\pi + tan^{-1}(-\omega_{\mathcal{C}ii}\mathcal{T}_{ii})}{\omega_{\mathcal{C}ii}T_{ii}} \tag{10}$$

The FOPDT models can be derived by solving Equations (8) - (10) with phase crossover frequencies.

III. CONTROLLER DESIGN

This section deals with the realization of the controller algorithm. The decentralized PID controller is designed by considering the nonlinear constraints. Further, the overshoot is reduced by imposing constraints on constraints on maximum amplitude closed-loop ratio $\mathcal{A}_r$. The FOPDT model $\mathcal{G}(s)$ can be expressed as

$$\mathcal{G}(s) = \frac{\mathcal{K}_{\mathcal{P}l}}{\mathcal{T}s + 1}e^{-\Phi s} \tag{11}$$

The transfer function of the PID controller $\mathcal{C}(s)$ is

$$\mathcal{C}(s) = \mathcal{K}_{\mathcal{C}l}\left(1 + \frac{1}{\mathcal{T}_{\mathcal{I}}s} + \mathcal{T}_{\mathcal{D}}s\right) \tag{12}$$

where $\mathcal{K}_{\mathcal{C}l}$, $\mathcal{T}_{\mathcal{I}}$, $\mathcal{T}_{\mathcal{D}}$ corresponds to the proportional gain, integral and derivative time constants respectively. Further,

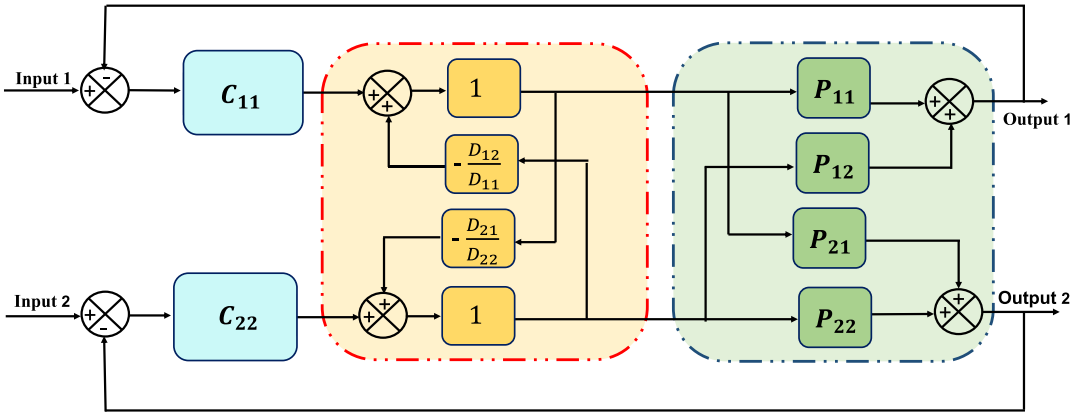

FIGURE 1. Decoupled TITO system.

from Equations (11) and (12), the open loop transfer function $\mathcal{W}_{\mathcal{O}}(s)$ is obtained as

$$\mathcal{W}_{\mathcal{O}}(s) = \frac{\mathcal{K}_{\mathcal{C}l}\mathcal{K}_{\mathcal{P}l}(\mathcal{T}_{\mathcal{I}}\mathcal{T}_{\mathcal{D}}s^2 + \mathcal{T}_{\mathcal{I}}s + 1)e^{-\Phi s}}{\mathcal{T}_{\mathcal{I}}s(\mathcal{T}s + 1)} \tag{13}$$

The phase change ($\varnothing_{\mathcal{O}}$) and amplitude ratio ($\vartheta_{\mathcal{O}}$) are obtained with frequency analysis to Equation (13), and is given as

$$\vartheta_{\mathcal{O}}(s) = \frac{\mathcal{K}_{\mathcal{C}l}\mathcal{K}_{\mathcal{P}l}\sqrt{(1-\omega^2\mathcal{T}_{\mathcal{I}}\mathcal{T}_{\mathcal{D}})^2 + (\omega\mathcal{T}_{\mathcal{I}}^2)}}{\omega\sqrt{\omega^2\mathcal{T}^2+1}\mathcal{T}_{\mathcal{I}}} \tag{14}$$

$$\varnothing_{\mathcal{O}} = \begin{cases} \Delta(\omega) - \omega\Phi - \tan^{-1}(\omega\mathcal{T}) - \dfrac{\pi}{2}, & if\ \Delta(\omega) \geq 0 \\ \Delta(\omega) - \omega\Phi - \tan^{-1}(\omega\mathcal{T}) + \dfrac{\pi}{2}, & if\ \Delta(\omega) < 0 \end{cases} \tag{15}$$

where

$$\Delta(\omega) = tan^{-1}\left(\frac{\omega\mathcal{T}_{\mathcal{I}}}{1-\omega^2\mathcal{T}_{\mathcal{I}}\mathcal{T}_{\mathcal{D}}}\right)$$

The closed loop transfer function $\mathcal{W}_{\mathcal{C}l}$ is

$$\mathcal{W}_{\mathcal{C}l} = \frac{\mathcal{W}_{\mathcal{O}}}{1+\mathcal{W}_{\mathcal{O}}}$$

Subsequently, the amplitude ratio $\vartheta_{\mathcal{C}l}$ is evaluated as

$$\vartheta_{\mathcal{C}l} = \frac{1}{\sqrt{(\frac{1}{\vartheta_{\mathcal{O}}} + cos\varnothing_{\mathcal{O}})^2 + sin^2\varnothing_{\mathcal{O}}}} \tag{16}$$

The phase crossover frequency $\vartheta_{\mathcal{C}l}(\omega_{\mathcal{C}})$ can be obtained as

$$\vartheta_{\mathcal{C}l}(\omega_{\mathcal{C}}) = 0.707 \tag{17}$$

The maximum value of closed-loop amplitude ratio $\mathcal{A}_r$ is

$$\mathcal{A}_r = max(\vartheta_{\mathcal{C}l}(\omega)), \forall\omega \tag{18}$$

The gain ($\mathcal{A}_m$) and phase margin ($\varnothing_m$) can be obtained from Equation (13) as

$$\mathcal{A}_m = \frac{1}{|\mathcal{W}_{\mathcal{O}}(j_{\omega_{\mathcal{P}}})|} \tag{19}$$

$$\varnothing_m = \angle\mathcal{W}_{\mathcal{O}}(j_{\omega_{\mathcal{G}}}) + \pi \tag{20}$$

where $||\mathcal{W}_{\mathcal{O}}(j_{\omega_{\mathcal{P}}})|| = 1$, $\angle\mathcal{W}_{\mathcal{O}}(j_{\omega_{\mathcal{G}}}) = -\pi$ and $\omega_{\mathcal{P}}$, $\omega_{\mathcal{G}}$ are the gain and phase crossover frequencies respectively. By substituting Equations (14) and (15) in Equations (19) and (20), the following equations are derived.

$$\mathcal{A}_m = \frac{\omega_{\mathcal{P}}\mathcal{T}_{\mathcal{I}}}{\mathcal{K}_{\mathcal{C}l}\mathcal{K}_{\mathcal{P}l}}\sqrt{\frac{\omega_{\mathcal{P}}^2\mathcal{T}^2+1}{(1-\omega_{\mathcal{P}}\mathcal{T}_{\mathcal{I}}\mathcal{T}_{\mathcal{D}})^2 + \omega_{\mathcal{P}}^2\mathcal{T}_{\mathcal{I}}^2}} \tag{21}$$

$$\varnothing_m = \begin{cases} \Delta(\omega_{\mathcal{G}}) - \omega_{\mathcal{G}}\Phi - \tan^{-1}(\omega_{\mathcal{G}}\mathcal{T}) - \dfrac{\pi}{2}, & if\ \Delta(\omega_{\mathcal{G}}) \geq 0 \\ \Delta(\omega_{\mathcal{G}}) - \omega_{\mathcal{G}}\Phi - \tan^{-1}(\omega_{\mathcal{G}}\mathcal{T}) + \dfrac{3\pi}{2}, & if\ \Delta(\omega_{\mathcal{G}}) < 0 \end{cases} \tag{22}$$

$$\frac{\mathcal{K}_{\mathcal{C}l}\mathcal{K}_{\mathcal{P}l}}{\omega_{\mathcal{G}}\mathcal{T}_{\mathcal{I}}}\sqrt{\frac{(1-\omega_{\mathcal{P}}^2\mathcal{T}_{\mathcal{I}}\mathcal{T}_{\mathcal{D}})^2 + (\omega_{\mathcal{G}}\mathcal{T}_{\mathcal{D}})^2}{\omega_{\mathcal{P}}^2\mathcal{T}^2+1}} = 1 \tag{23}$$

$$\varnothing_p = \begin{cases} \Delta(\omega_{\mathcal{P}}) - \omega_{\mathcal{P}}\Phi - \tan^{-1}(\omega_{\mathcal{P}}\mathcal{T}) - \dfrac{\pi}{2}, & if\ \Delta(\omega_{\mathcal{P}}) \geq 0 \\ \Delta(\omega_{\mathcal{P}}) + \omega_{\mathcal{P}}\Phi + \tan^{-1}(\omega_{\mathcal{P}}\mathcal{T}) + \dfrac{3\pi}{2}, & if\ \Delta(\omega_{\mathcal{P}}) < 0 \end{cases} \tag{24}$$

Due to the existence of unknown factors $\omega_{\mathcal{G}}$, $\omega_{\mathcal{P}}$, $\mathcal{K}_{\mathcal{C}l}$, $\mathcal{T}_{\mathcal{I}}$ and $\mathcal{T}_{\mathcal{D}}$, Equations (21) - (24) can not be solved directly. Hence, a constraint is imposed on maximum closed loop bandwidth, maximum amplitude ratio, gain and phase margins to formulate the optimization problem and is given by

Theorem 1:

$$\max_{\omega_{\mathcal{G}},\omega_{\mathcal{P}},\mathcal{K}_{\mathcal{C}l},\mathcal{K}_{\mathcal{P}l},\mathcal{T}_{\mathcal{I}},\mathcal{T}_{\mathcal{D}}} \omega_{\mathcal{C}}$$

subjected to

$$\begin{aligned} \vartheta_{\mathcal{C}l}(\omega_{\mathcal{C}}) &= 0.707 \\ \mathcal{A}_m &\geq \mathcal{A}_m^* \\ \varnothing_m &\geq \varnothing_m^* \\ \mathcal{A}_r &\leq \gamma_m^* \end{aligned}$$

where $\mathcal{A}_m^*$ and $\varnothing_m^*$ are lower bounds of gain and phase margin respectively and γ_m^* corresponds to upper bound maximum

amplitude ratio. However, $\mathcal{A}_m$ and $\varnothing_m$ are related to gain and phase margin bounds as reported in [51] and are given as

$$\mathcal{A}_m \geq 1 + \frac{1}{\mathcal{A}_r} \tag{25}$$

$$\varnothing_m \geq 2sin^{-1}\left(\frac{1}{2\mathcal{A}_r}\right) \tag{26}$$

Lemma 1: Equations (25) and (26) depicts the dependence of $\mathcal{A}_r$ and gain and phase margins.

Lemma 2: It can be inferred that a low value for γ_m^* corresponds to a high value for $\mathcal{A}_m$ and γ_m^* comparing to $\mathcal{A}_m^*$ and is achieved in a more robust or less aggressive manner.

Lemma 3: The maximum value of ϑ_{Cl} needs to be determined to find $\mathcal{A}_r$ in the frequency range (0,∞).

Lemma 4: To resolve the optimization problem, a new term $\omega_{\mathcal{MAX}}$ needs to be considered as $\omega_{\mathcal{C}}$ is unknown.

The MatLab optimization tool "fmincon" is used to determine the unknowns in Equations (21) - (24).

IV. ANALYSIS OF STABILITY AND ROBUSTNESS

This section describes the stability and robustness analysis of the TITO system.

A. STABILITY ANALYSIS

Due to the nonlinear property, the stability analysis of the MIMO process is very difficult. The open-loop transfer function is

$$\mathcal{W}_{\mathcal{O}}(s) = \mathcal{C}(s)\mathcal{G}(s) \tag{27}$$

Besides, the closed loop characteristics polynomial can be obtained as

$$det[I + \mathcal{C}(s)\mathcal{G}(s)] = 0 \tag{28}$$

where $\mathcal{C}(s)$ is the PID controller with two terms $c_1^*(s)$ (control input to tank 1)and $c_2^*(s)$ (control input to tank 2). Further, $\mathcal{C}_t(s)$ can be expressed as

$$\mathcal{C}(s) = \begin{bmatrix} c_1^*(s) & 0 \\ 0 & c_2^*(s) \end{bmatrix} \tag{29}$$

For the coupled tank systems, the closed-loop characteristics polynomial described in the Equation (28), is expressed as

$$As^4 + Bs^3 + Cs^2 + Ds + 1 = 0 \tag{30}$$

As discussed in [52], the system stability can be verified from the Routh array of Equation (30). Further, by considering the boundary values, Equation (30) is modified as

$$\begin{bmatrix} p_4 & q_4 \end{bmatrix} s^4 + \begin{bmatrix} p_3 & q_3 \end{bmatrix} s^3 + \begin{bmatrix} p_2 & q_2 \end{bmatrix} s^2 + \begin{bmatrix} p_1 & q_1 \end{bmatrix} s + \begin{bmatrix} p_0 & q_0 \end{bmatrix} = 0 \tag{31}$$

Further, the four Kharitonov polynomials $\mathcal{K}^1(s)$, $\mathcal{K}^2(s)$, $\mathcal{K}^3(s)$, $\mathcal{K}^4(s)$ can be derived as

$$\mathcal{K}^1(s) = p_0 + p_1 s + q_2 s^2 + q_3 s^3 + p_4 s^4 \tag{32}$$

$$\mathcal{K}^2(s) = p_0 + q_1 s + q_2 s^2 + p_3 s^3 + p_4 s^4 \tag{33}$$

$$\mathcal{K}^3(s) = q_0 + p_1 s + p_2 s^2 + q_3 s^3 + q_4 s^4 \tag{34}$$

$$\mathcal{K}^4(s) = q_0 + q_1 s + p_2 s^2 + p_3 s^3 + q_4 s^4 \tag{35}$$

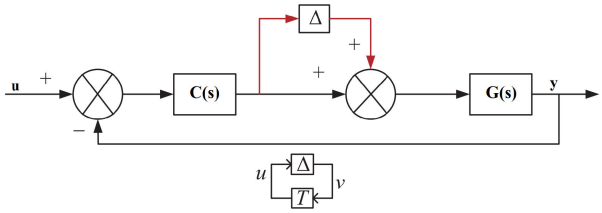

FIGURE 2. Schematics of multiplicative-input uncertainty.

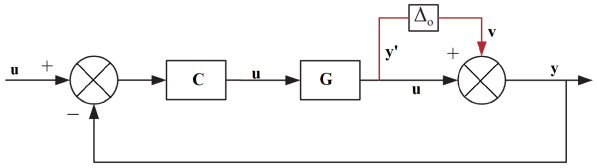

FIGURE 3. Schematics of multiplicative-output uncertainty.

For the first Kharitonov polynomial $\mathcal{K}^1(s)$, the Hurwitz matrix $\mathcal{HM}$ and the row reduced Hurwitz matrix $\mathcal{HM}_n$ is given by

$$\mathcal{HM} = \begin{bmatrix} p_1 & p_0 & 0 & 0 \\ p_3 & p_2 & p_1 & p_0 \\ 0 & p_4 & p_3 & p_2 \\ 0 & 0 & 0 & p_4 \end{bmatrix} \tag{36}$$

$$\mathcal{HM}_n = \begin{bmatrix} p_{11} & p_{12} & 0 & 0 \\ 0 & p_{22} & \cdots & \cdots \\ \cdots & \cdots & \cdots & \cdots \\ 0 & 0 & 0 & p_{44} \end{bmatrix} \tag{37}$$

Similarly, the Hurwitz matrix $\mathcal{HM}$ and the row reduced Hurwitz matrix $\mathcal{HM}_n$ is derived for the other Kharitonov polynomials $\mathcal{K}^2(s)$, $\mathcal{K}^3(s)$ and $\mathcal{K}^4(s)$. As reported in [53], if there is any sign change in the diagonal elements of $\mathcal{HM}_n$, the system is not Hurwitz stable. Besides, if all four polynomials are Hurwitz stable, the system will be robustly stable. The analysis is given in the Appendix section.

B. ANALYSIS OF ROBUSTNESS

The robustness analysis of the controller is essential because of the unmodeled process dynamics. Uncertainties affect the system stability and hence, both multiplicative input, as well as output uncertainties, are considered to analyze the stability. The schematics of input and output uncertainties are denoted by Figures 2 and 3 respectively. The $T-\Delta$ form of the transfer function of the system is given

$$T_{MI} = -\mathcal{C}(I + \mathcal{GC})^{-1}\mathcal{G} \tag{38}$$

$$T_{MO} = -\mathcal{GC}(I + \mathcal{GC})^{-1} \tag{39}$$

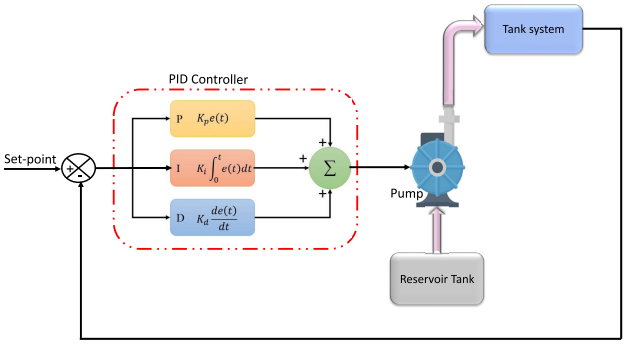

FIGURE 4. Tank system level control.

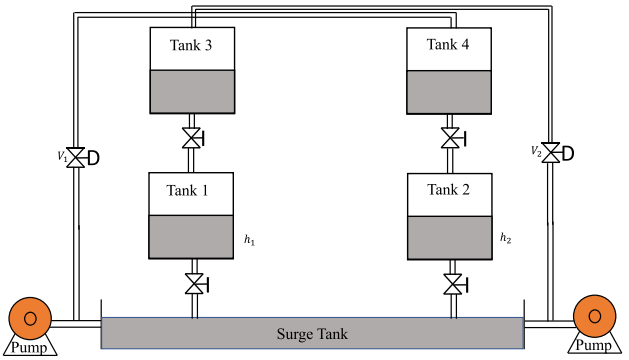

FIGURE 5. QTS.

As presented in [50], [55], and [57], robustness can be attained only if the following criteria are achieved.

$$||T_{MI}||_\infty < \frac{1}{||\Delta_I||_\infty} \tag{40}$$

$$||T_{MO}||_\infty < \frac{1}{||\Delta_O||_\infty} \tag{41}$$

However, more time is required to evaluate Equation (40) and (41). Hence, to reduce the computational time, an equivalent relationship is formed using the small gain theorem and the spectral radius stability as reported in [50] as

$$\rho(\mathcal{C}(I+\mathcal{GC})^{-1}G\Delta_I) < 1 \; \forall \; \omega \; \varepsilon \; [0 \;\; \infty] \tag{42}$$

$$\rho(\mathcal{GC}(I+\mathcal{GC})^{-1}G\Delta_O) < 1 \; \forall \; \omega \; \varepsilon \; [0 \;\; \infty] \tag{43}$$

The stability is analyzed by evaluating the magnitude plots Equations (42) and (43) to determine whether it is under unity or not for $\omega \;\; \varepsilon \;\; [0 \;\; \infty]$.

V. SIMULATION RESULTS

The simulation results of the proposed control scheme are analyzed in this section by using Matlab/Simulink environment. Further, the performance of the controller is evaluated for robustness. The typical level control system is illustrated in Figure 4. The objective is to maintain the tank system at the desired level. The following variable area coupled tank systems were considered quadruple tank system (QTS) [44], and coupled spherical tank system (CSTS) [31] coupled conical tank system (CCTS) [43].

A. QUADRUPLE TANK SYSTEM

The schematic diagram of the QTS is shown in Figure 5. The levels of tanks 1 and 2 (h_1 and h_2) need to be controlled.

As reported in [44], the transfer function $\mathcal{G}(s)$ is given by

$$\mathcal{G}(s) = \begin{bmatrix} \frac{0.834e^{-5s}}{6.57s+1} & \frac{1.39e^{-7s}}{(10.231s+1)(6.57s+1)} \\ \frac{1.271e^{-9s}}{(14.05s+1)(11.29s+1)} & \frac{0.757e^{-6s}}{11.29s+1} \end{bmatrix} \tag{44}$$

Referring to Equation (2), the decouplers $\mathcal{D}(s)$ can be obtained as

$$\mathcal{D}(s) = \begin{bmatrix} 0 & \frac{-1.67}{10.23s+1}e^{-2s} \\ \frac{-1.678}{14.05s+1}e^{-3s} & 0 \end{bmatrix} \tag{45}$$

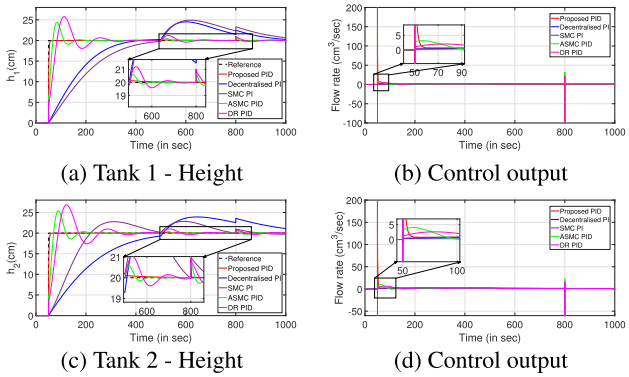

(a) Tank 1 - Height (b) Control output

(c) Tank 2 - Height (d) Control output

FIGURE 6. Servo and regulatory response.

From Equations (8) - (10), the FOPDT model $\mathcal{G}_{ii}(s)$ can be derived as

$$\mathcal{G}_{11}(s) = \frac{2.332}{86.35s+1}e^{-0.069s} \tag{46}$$

$$\mathcal{G}_{22}(s) = \frac{2.119}{110.65s+1}e^{-0.061s} \tag{47}$$

The decentralized PID controller $\mathcal{C}(s)$ satisfying the design specifications is derived from Equation (25)

$$\mathcal{C}(s) = \begin{bmatrix} 28 + \frac{0.285}{s} + 7.82s & 0 \\ 0 & 37.5 + \frac{0.305}{s} + 11.5s \end{bmatrix} \tag{48}$$

Figure 6 presents the response for maintaining the level of the QTS. The main aim is to maintain the level of the tank at 20 cm. The proposed controller is able to meet the design requirements at a faster rate with minimal control effort than the controllers reported in the literature: disturbance-rejection-PID controller (DR-PID) [24], sliding-mode-PI (SMC-PI) controller [49], decentralized PI controller [47], and adaptive-SMC-PID (ASMC PID) controller [49]. Further, for verifying the regulatory response, a step signal is injected as input (500 seconds) and output (800 seconds) disturbance respectively. The set-point tracking is illustrated by Figures 6a and 6c. The corresponding controller outputs are shown in Figures 6b and 6d. A comparative analysis is presented in Table 1 by evaluating the performance indexes like integral time absolute error (ITAE), integral absolute error (IAE), and integral squared error (ISE). It can be inferred that

TABLE 1. Quadruple tank system - performance indexes.

Control Method	u-y	Servo Response 0 - 500 seconds			Regulatory Response 500 - 1000 seconds		
		IAE	ISE	ITAE	IAE	ISE	ITAE
Proposed PID	h_1	6.96	32.81	432.7	52.42	235	1.55×10^4
	h_2	7.31	36.5	433.5	45.19	241.6	1.10×10^4
Decentralized PI [47]	h_1	1131	6611	1.57×10^5	3436	3.01×10^4	1.11×10^6
	h_2	1559	8904	2.723×10^5	4461	3.97×10^4	1.53×10^6
SMC PI [49]	h_1	1440	8496	2.32×10^5	4335	3.91×10^4	1.5×10^6
	h_2	1021	5486	1.60×10^5	2590	2.3×10^4	6.75×10^5
ASMC PID [49]	h_1	138	420.9	1.09×10^4	310.1	1696	4.4×10^4
	h_2	192	626.4	1.67×10^4	425.9	2590	6.1×10^4
DR PID [24]	h_1	332.4	1090	3.79×10^4	776.5	4426	1.5×10^5
	h_2	452.5	1569	5.92×10^5	1027	6342	2.1×10^5

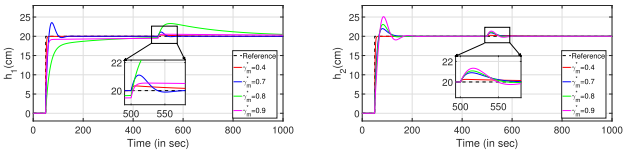

(a) Tank 1 - Height (b) Tank 2 - Height

FIGURE 7. Servo and regulatory response for various values of γ_m^*.

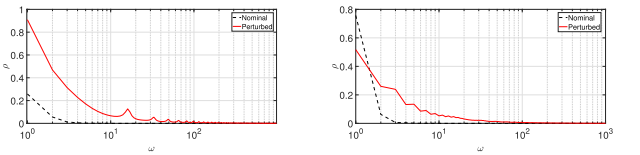

(a) Multiplicative input uncertainty (b) Multiplicative output uncertainty

FIGURE 8. Spectral radius plot.

the proposed control algorithm is better than the techniques mentioned in the aforementioned literature.

As mentioned in Lemma 2, the γ_m^* values affect the closed-loop response of the system. From Figure 7 it is inferred that the low values of γ_m^* result in better servo and regulatory responses. The servo and regulatory response for the variation of level in tanks 1 and 2 are shown by Figures 7a and 7b respectively.

1) ANALYSIS OF ROBUSTNESS

The magnitude plots for analyzing the robustness criteria described in Equations (42) and (43) are shown in Figure 8. It can be inferred from the figure that robust stability criteria is attained. Besides, the transient response of the system (Figure 9) is considered for the robustness study. Referring to Figures 2 and 3, a white noise of power 25 is applied. Figures 9a and 9b denote the response of the system with input uncertainties while Figures 9c and 9d denote the output uncertainty. Further, the FOPDT model parameters mentioned in Equations (46) and (47) are subjected to a change of ±10%, ±20% and ±30% variations from the normal values to prove the robustness of the proposed control law. The response is shown in Figure 10. Figures 10a and 10b shows the ±10%, ±20% and ±30% variation of Equation (46). Similarly, Figures 10c and 10d shows the corresponding variation of Equation (47).

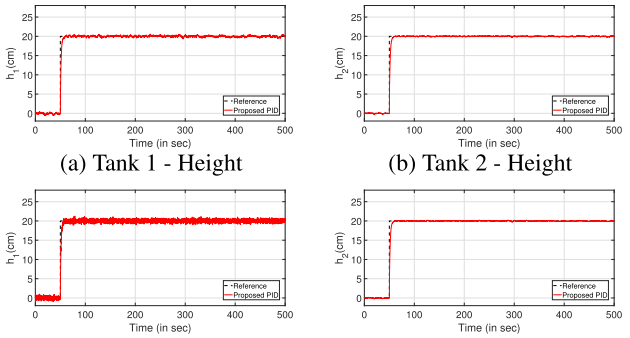

(a) Tank 1 - Height (b) Tank 2 - Height
(c) Tank 1 - Height (d) Tank 2 - Height

FIGURE 9. Set-point tracking of input and output uncertainties.

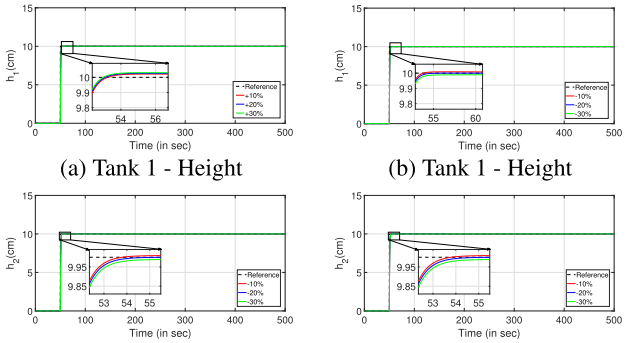

(a) Tank 1 - Height (b) Tank 1 - Height
(c) Tank 2 - Height (d) Tank 2 - Height

FIGURE 10. Set-point tracking of Equations (46) and (47) for parametric variations.

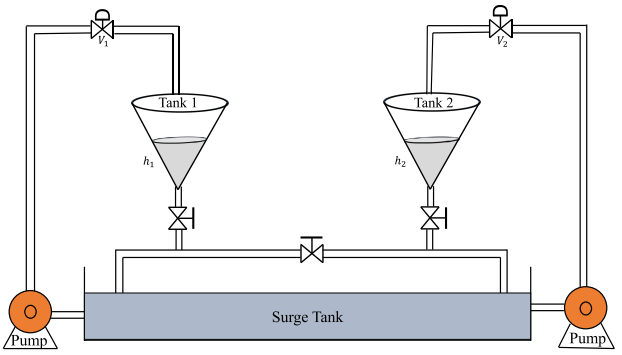

FIGURE 11. CCTS.

B. COUPLED CONICAL TANK SYSTEM

Figure 11 presents the schematics of the CCTS where the levels are denoted as h_1 and h_2. Article [43] describes the transfer function $\mathcal{G}(s)$ of CCTS as

$$\mathcal{G}(s) = \begin{bmatrix} \frac{1.8361\, e^{-11.5s}}{340.7s+1} & \frac{0.723\, e^{-19.2s}}{415.4s+1} \\ \frac{0.74\, e^{-19.1s}}{407.3s+1} & \frac{1.89\, e^{-12.4s}}{365.6s+1} \end{bmatrix} \tag{49}$$

Further, Equation (2) describes the designed decouplers $\mathcal{D}(s)$ as

$$\mathcal{D}(s) = \begin{bmatrix} 0 & \frac{-(246.33s+0.73)}{762.72s+1.84} e^{-s} \\ \frac{-(270.55s+0.74)}{770.91s+1.89} e^{-6.7s} & 0 \end{bmatrix} \tag{50}$$

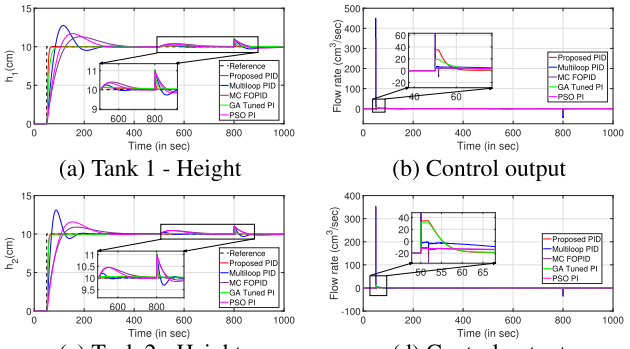

(a) Tank 1 - Height (b) Control output

(c) Tank 2 - Height (d) Control output

FIGURE 12. Servo and regulatory response.

TABLE 2. Coupled conical tank system- performance indexes.

Control Method	u-y	Servo Response 0 - 500 seconds			Regulatory Response 500 - 1000 seconds		
		IAE	ISE	ITAE	IAE	ISE	ITAE
Proposed PID	h_1	6.96	32.81	432.7	83.85	346.4	2.4 X 10^4
	h_2	7.31	36.5	433.5	69.19	365.8	1.7 X 10^4
Multiloop PID [43]	h_1	1131	6611	1.57 X 10^5	390.7	1365	7.3 X 10^4
	h_2	1559	8904	2.72 X 10^5	245.3	904.7	4.01 X 10^4
MCFOPID [43]	h_1	1440	8496	2.32X 10^5	553.7	1904	1.2 X 10^5
	h_2	1021	5486	1.60 X 10^5	447.8	1507	1.03 X 10^5
GA PI [25]	h_1	138	420.9	1.09 X 10^4	150.8	560.6	4.1 X 10^4
	h_2	192	626.4	1.67 X 10^4	114.3	380.1	3.2 X 10^5
PSO PI [46]	h_1	332.4	1090	3.79 X 10^4	485.2	1730	1.02 X 10^5
	h_2	452.5	1569	5.92 X 10^4	481.5	1732	1.04 X 10^5

Furthermore, Equations (51) and (52) presents the FOPDT model $\mathcal{G}_{ii}(s)$ as

$$\mathcal{G}_{11}(s) = \frac{1.54}{268.99s+1}e^{-1.54s} \tag{51}$$

$$\mathcal{G}_{22}(s) = \frac{1.598}{211.9s+1}e^{-1.85s} \tag{52}$$

Thus, the proposed decentralized PID controller $\mathcal{C}(s)$is

$$\mathcal{C}(s) = \begin{bmatrix} 35 + \frac{1.151}{s} + 2.03s & 0 \\ 0 & 23 + \frac{1.123}{s} + 3.03s \end{bmatrix} \tag{53}$$

In order to prove the effectiveness of the proposed control algorithm for the CCTS, simulations were conducted. Figure 12 presents the servo and regulatory responses of the CCTS system. It can be inferred from the figure that the proposed controller exhibits better set-point tracking by reducing the overshoot and settling time than multiloop PID [25], multivariable-centralized FOPID (MCFOPID) [25], PI controllers based on particle-swarm-optimization (PSO) [46] and genetic-algorithm (GA) [43]. Similarly, the regulatory response is verified with a step signal as input (500 seconds) and output (800 seconds) disturbance. The set-point tracking is shown in Figures 12a and 12c and Figures 12b and 12d presents the corresponding controller outputs. Further, the Performance Indexes of the controllers are listed in Table 2.

Subsequently, the dependency of the γ_m^* in the transient response is shown in Figure 13. Figures 13a and 13b show the level variations of tanks 1 and 2 respectively.

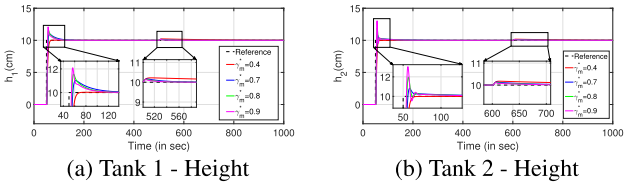

(a) Tank 1 - Height (b) Tank 2 - Height

FIGURE 13. Servo and regulatory response for various values of γ_m^*.

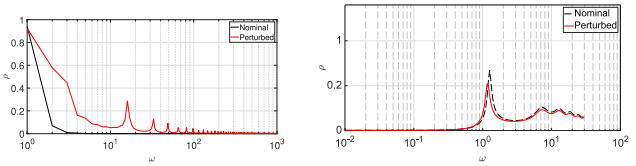

(a) Multiplicative input uncertainty (b) Multiplicative output uncertainty

FIGURE 14. Spectral radius plot.

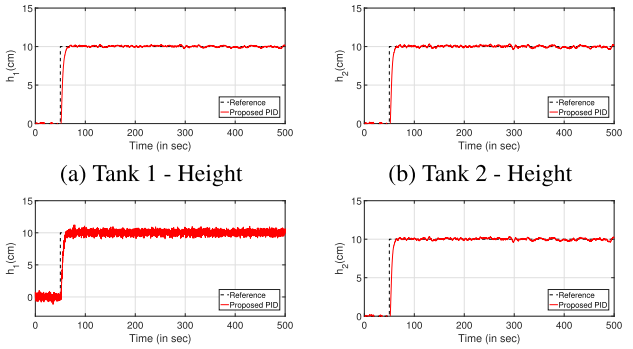

(a) Tank 1 - Height (b) Tank 2 - Height

(c) Tank 1 - Height (d) Tank 2 - Height

FIGURE 15. Set-point tracking of input and output uncertainties.

1) ANALYSIS OF ROBUSTNESS

Similarly, the robustness criteria described in Equations (42) and (43) is presented in Figure 14. The stability criteria is satisfied. Further, Figure 15 verifies the robustness of the proposed controller with the white noise of power 35. The input uncertainties are shown by Figures 15a and 15b while Figures 15c and 15d show the output uncertainty. Further, the model parameters mentioned in Equation (51) and (52) are varied by ±10%, ±20% and ±30%. Figures 16a and 16b show the ±10%, ±20% and ±30% variation of (51) while Figures 16c and 16d shows the variation of (52).

C. COUPLED SPHERICAL TANK SYSTEM

The schematics of the CSTS are illustrated in Figure 17 where h_1, h_2 needs to be regulated. The process transfer function of CSTS $\mathcal{G}(s)$ as presented in [31] is

$$\mathcal{G}(s) = \begin{bmatrix} \frac{0.143e^{-0.996s}}{236.25s+1} & \frac{0.13e^{-82.305s}}{723.305s+1} \\ \frac{0.13e^{-82.305s}}{723.305s+1} & \frac{0.16e^{-0.996s}}{314.47s+1} \end{bmatrix} \tag{54}$$

Subsequently, the designed decouplers $\mathcal{D}(s)$ are

$$\mathcal{D}(s) = \begin{bmatrix} 0 & -\frac{(30.72s+0.13)}{103.43s+0.143}e^{-81.31s} \\ \frac{(40.88s+0.13)}{115.73s+0.16}e^{-81.31s} & 0 \end{bmatrix} \tag{55}$$

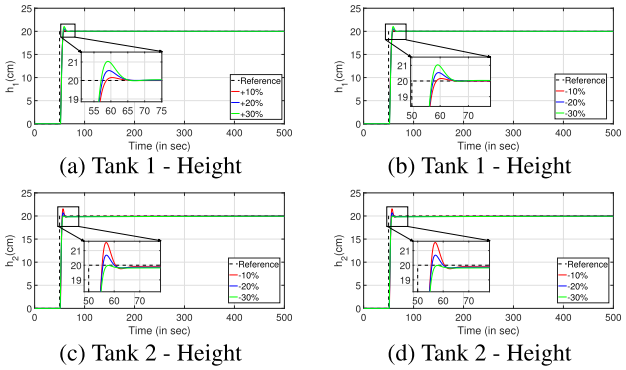

(a) Tank 1 - Height (b) Tank 1 - Height

(c) Tank 2 - Height (d) Tank 2 - Height

FIGURE 16. Set-point tracking of Equations (51) and (52) for parametric variations.

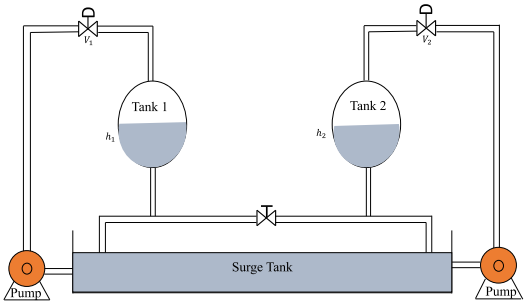

FIGURE 17. CSTS.

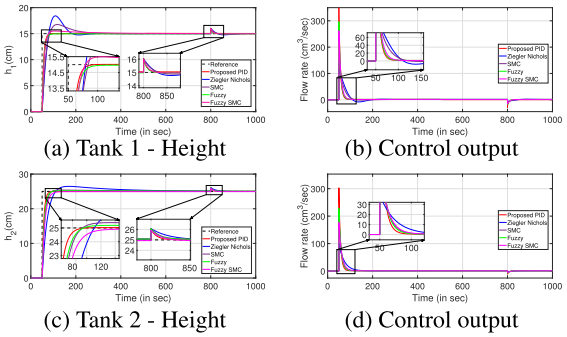

(a) Tank 1 - Height (b) Control output

(c) Tank 2 - Height (d) Control output

FIGURE 18. Servo and regulatory response.

TABLE 3. Coupled spherical tank system - performance indexes.

Control Method	u-y	Servo Response 0 - 500 seconds			Regulatory Response 500 - 1000 seconds		
		IAE	ISE	ITAE	IAE	ISE	ITAE
Proposed PID	h_1	6.962	32.81	432.7	343.4	850.3	1.31 X 10^4
	h_2	7.311	36.5	433.5	420.4	2341	1.45 X 10^4
Ziegler Nichols [31]	h_1	1131	6611	1.571 X 10^5	425.4	2279	6.03 X 10^4
	h_2	1559	8904	2.723 X 10^5	867.6	6718	1.71 X 10 4
Sliding Mode [31]	h_1	1440	8496	2.32X 10^5	376.6	1804	5.73 X 10^4
	h_2	1021	5486	1.606 X 10^5	425.1	3348	8.9 X 10^4
Fuzzy PID [30]	h_1	138	420.9	1.09 X 10^4	149.5	881.2	2.5 X 10^4
	h_2	192	626.4	1.67 X 10^4	339.1	2969	6.74 X 10^4
Fuzzy SMC [12]	h_1	332.4	1090	3.791 X 10^4	230.3	988.5	4.17 X 10^4
	h_2	452.5	1569	5.927 X 10^4	379.2	3846	5.93 X 10^4

Besides, the FOPDT model $\mathcal{G}_{ii}(s)$ is

$$\mathcal{G}_{11}(s) = \frac{0.1056}{160.5s+1}e^{-0.108s} \tag{56}$$

$$\mathcal{G}_{22}(s) = \frac{0.118}{203.6s+1}e^{-0.091s} \tag{57}$$

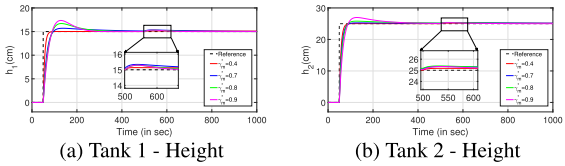

(a) Tank 1 - Height (b) Tank 2 - Height

FIGURE 19. Servo and regulatory response for various values of γ_m^*.

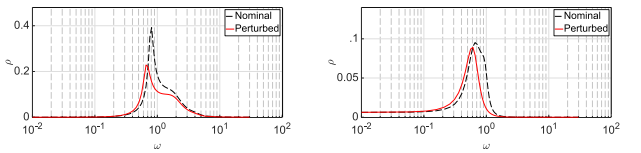

(a) Multiplicative input uncertainty (b) Multiplicative output uncertainty

FIGURE 20. Spectral radius plot.

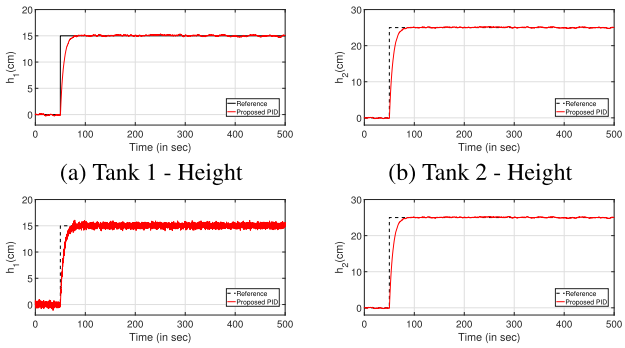

(a) Tank 1 - Height (b) Tank 2 - Height

(c) Tank 1 - Height (d) Tank 2 - Height

FIGURE 21. Set-point tracking of input and output uncertainties.

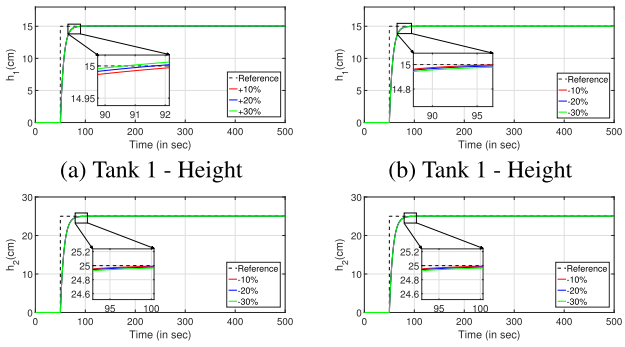

(a) Tank 1 - Height (b) Tank 1 - Height

(c) Tank 2 - Height (d) Tank 2 - Height

FIGURE 22. Set-point tracking of Equations (56) and (57) for parametric variations.

The proposed decentralized PID controller $\mathcal{C}(s)$ is

$$\mathcal{C}(s) = \begin{bmatrix} 12.5 + \frac{0.8}{s} + 1.5s & 0 \\ 0 & 32.1 + \frac{5.5}{s} + 2.3s \end{bmatrix} \tag{58}$$

Similarly, Figure 19 shows the set-point point tracking for the CSTS. The design specifications can be easily attained when compared to [12], [30], and [31]. Similarly, Table 3 highlights the efficiency of the proposed control law. Besides, the effect of the γ_m^* is shown by Figure 19.

1) ANALYSIS OF ROBUSTNESS

Subsequently, the robustness criteria described in Equations (42) and (43) is shown in Figure 20.The robust stability criteria is satisfied. Besides, the robustness is analyzed in Figure 21 wherein a noise signal of power 45 is applied as input and output disturbance. Further, the model parameters mentioned in Equations (56) and (57) are changed by ±10%, ±20% and ±30%. The corresponding reference tracking is shown in Figure 22.

VI. CONCLUSION

A decentralized PID controller for various variable area-coupled tank systems based on non-linear constraint optimization is presented in this paper. Albeit, the robustness can be analyzed with the specifications of gain and phase margin, design flexibility is the main highlight of the proposed control law. Further, the PID controller parameters were derived by imposing constraints on the closed-loop amplitude ratio thereby ensuring reference tracking and robustness. The FOPDT models were derived for different coupled tank systems. Besides, the loop interactions were reduced by designing decouplers. Further, the robustness is verified with multiplicative input and output uncertainties. Furthermore, the effect of parametric variations is also studied. Additionally, the stability is analyzed with the Kharitonov-Hurwitz theorem. From the simulation results, it can be inferred that the proposed controller is able to attain the design specifications and exhibits more robust characteristics than the existing techniques presented in the aforementioned literature.

APPENDIX

QUADRUPLE TANK SYSTEM

The FOPDT model of the plant $\mathcal{G}(s)$

$$\mathcal{A}(s) = \begin{bmatrix} \frac{2.332}{86.35s+1}e^{-0.069s} & 1 \\ 1 & \frac{2.119}{110.659s+1}e^{-0.061s} \end{bmatrix} \tag{59}$$

The designed PID controller $\mathcal{C}(s)$ is

$$\mathcal{C}(s) = \begin{bmatrix} 28 + \frac{0.2985}{s} + 7.82s & 0 \\ 0 & 37.5 + \frac{0.305}{s} + 11.5s \end{bmatrix} \tag{60}$$

Hence, as per Equation (27), the open-loop transfer function $\mathcal{W}_0(s)$ can be obtained as

$$\mathcal{W}_0(s) = \mathcal{C}(s) * \mathcal{G}(s) = \begin{bmatrix} 28 + \frac{0.2985}{s} + 7.82s & 0 \\ 0 & 37.5 + \frac{0.305}{s} + 11.5s \end{bmatrix} * \begin{bmatrix} \frac{2.332}{86.35s+1}e^{-0.069s} & 1 \\ 1 & \frac{2.119}{110.659s+1}e^{-0.061s} \end{bmatrix} \tag{61}$$

where, the time delays can be expressed by neglecting the higher order terms as $e^{-0.069s} = 1 - 0.069s$ and $e^{-0.061s} = 1 - 0.061s$. Further, Equations (59) and (61) can be rearranged as

$$\mathcal{A}(s) = \begin{bmatrix} \frac{2.332-0.16s}{86.35s+1} & 1 \\ 1 & \frac{2.119-0.3s}{110.65s+1} \end{bmatrix} \tag{62}$$

$$\mathcal{W}_0(s) = \begin{bmatrix} \frac{7.82s^2+28s+0.285}{s} & 0 \\ 0 & \frac{11.5s^2+37.5s+0.305}{s} \end{bmatrix} * \begin{bmatrix} \frac{2.332-0.16s}{86.35s+1} & 1 \\ 1 & \frac{2.119-0.3s}{110.65s+1} \end{bmatrix} \tag{63}$$

$$= \begin{bmatrix} \frac{-1.25s^3+13.73s^2-65.25s+0.66}{86.35s^2+s} & \frac{7.82s^2+28s+0.285}{s} \\ \frac{11.5s^2+37.5s+0.305}{s} & \frac{-1.5s^3+19.57s^2-79.4s+0.65}{110.65s^2+s} \end{bmatrix} \tag{64}$$

As described in Equation (28),

$$det[I + \mathcal{C}(s)\mathcal{A}(s)] = 0 \tag{65}$$

On substituting, Equations (64) into (65), the characteristics Equation can be obtained as

$$859.2s^6 + 589.7s^5 + 101.9s^4 + 408.5s^3 + 485.8s^2 + 129.9s + 0.3421 = 0 \tag{66}$$

The four Kharitonov polynomials $\mathcal{K}^1(s)$, $\mathcal{K}^2(s)$, $\mathcal{K}^3(s)$, $\mathcal{K}^4(s)$ are derived from Equations (32) - (35) as

$$\mathcal{K}^1(s) = s^6 + 31.06s^5 + 116.18s^4 + 119.09s^3 + 297.86s^2 + 141.035s + 205.585 \tag{67}$$

$$\mathcal{K}^2(s) = s^6 + 46.409s^5 + 173.56s^4 + 119.0s^3 + 297.86s^2 + 210.779s + 307.109 \tag{68}$$

$$\mathcal{K}^3(s) = s^6 + 37.97s^5 + 173.56s^4 + 145.44s^3 + 173.56s^2 + 379.7s + 307.109 \tag{69}$$

$$\mathcal{K}^4(s) = s^6 + 37.97s^5 + 116.18s^4 + 97.68s^3 + 297.86s^2 + 172.376s + 205.85 \tag{70}$$

The Hurwitz matrix and the row-reduced Hurwitz matrices for the Kharitonov polynomials described in Equations (67) - (70) are given by Table 4. The elements in the matrix are positive and there is no sign change. The positive values of the diagonal elements are verified and the proposed controller is robust stable.

TABLE 4. Hurwitz matrix and row reduced Hurwitz matrix - QTS.

Polynomial	HM	HM_n	Comments
$\mathcal{K}^1(s)$	$\begin{bmatrix} 46.4 & 1 & 0 & 0 & 0 & 0 \\ 119 & 116.2 & 31 & 1 & 0 & 0 \\ 141 & 297.8 & 119 & 116.2 & 31 & 0 \\ 0 & 205.5 & 141 & 297.8 & 119 & 116.2 \\ 0 & 0 & 0 & 205.5 & 141 & 297.8 \\ 0 & 0 & 0 & 0 & 0 & 205.5 \end{bmatrix}$	$\begin{bmatrix} 46.4 & 1 & 0 & 0 & 0 & 0 \\ 0 & 112 & 310 & 0 & 0 & 0 \\ 0 & 0 & 111 & 115 & 310 & 0 \\ 0 & 0 & 0 & 208.3 & 117 & 116.2 \\ 0 & 0 & 0 & 0 & 101 & 848.5 \\ 0 & 0 & 0 & 0 & 0 & 101 \end{bmatrix}$	Hurwitz stable
$\mathcal{K}^2(s)$	$\begin{bmatrix} 46.4 & 1 & 0 & 0 & 0 & 0 \\ 119 & 173.5 & 46.4 & 0 & 0 & 0 \\ 210.8 & 297.8 & 119 & 173.5 & 46.4 & 0 \\ 0 & 307.1 & 210.8 & 297.8 & 119 & 173.5 \\ 0 & 0 & 0 & 307.1 & 210.8 & 297.8 \\ 0 & 0 & 0 & 0 & 0 & 307.1 \end{bmatrix}$	$\begin{bmatrix} 46.4 & 1 & 0 & 0 & 0 & 0 \\ 0 & 170.9 & 46.4 & 0 & 0 & 0 \\ 0 & 0 & 111.4 & 173.3 & 464.5 & 0 \\ 0 & 0 & 0 & 97.8 & 114.1 & 173.5 \\ 0 & 0 & 0 & 0 & 337.2 & 51.5 \\ 0 & 0 & 0 & 0 & 0 & 307.1 \end{bmatrix}$	Hurwitz stable
$\mathcal{K}^3(s)$	$\begin{bmatrix} 37.9 & 1 & 0 & 0 & 0 & 0 \\ 145.44 & 173.5 & 379.9 & 1 & 0 & 0 \\ 37.97 & 173.5 & 145.4 & 173.5 & 37.9 & 0 \\ 0 & 307.1 & 37.9 & 173.5 & 145.4 & 173.5 \\ 0 & 0 & 0 & 307.1 & 37.9 & 173.5 \\ 0 & 0 & 0 & 0 & 0 & 307.1 \end{bmatrix}$	$\begin{bmatrix} 37.9 & 1 & 0 & 0 & 0 & 0 \\ 0 & 169.7 & 37.9 & 1 & 0 & 0 \\ 0 & 0 & 142 & 173.4 & 37.9 & 0 \\ 0 & 0 & 0 & 25.1 & 147.69 & 173.5 \\ 0 & 0 & 0 & 0 & 180.3 & 195 \\ 0 & 0 & 0 & 0 & 0 & 307.1 \end{bmatrix}$	Hurwitz stable
$\mathcal{K}^4(s)$	$\begin{bmatrix} 37.9 & 1 & 0 & 0 & 0 & 0 \\ 97.6 & 116.1 & 37.9 & 0 & 0 & 0 \\ 172.3 & 297.8 & 97.6 & 116.1 & 37.9 & 0 \\ 0 & 205.8 & 172.3 & 297.8 & 97.6 & 116.1 \\ 0 & 0 & 0 & 205.8 & 172.3 & 297.8 \\ 0 & 0 & 0 & 0 & 0 & 205.8 \end{bmatrix}$	$\begin{bmatrix} 37.9 & 1 & 0 & 0 & 0 & 0 \\ 0 & 113.6 & 37.91 & 1 & 0 & 0 \\ 0 & 0 & 87.8 & 115.9 & 397.7 & 0 \\ 0 & 0 & 0 & 159.3 & 93.2 & 116.1 \\ 0 & 0 & 0 & 0 & 103.4 & 120.1 \\ 0 & 0 & 0 & 0 & 0 & 1.4 \end{bmatrix}$	Hurwitz stable

TABLE 5. Hurwitz matrix and row reduced Hurwitz matrix - CSTS.

Polynomial	HM	HM_n	Comments
$\mathcal{K}^1(s)$	$\begin{bmatrix} 34.1 & 1 & 0 & 0 & 0 & 0 \\ 84.1 & 37.6 & 34.1 & 1 & 0 & 0 \\ 53.6 & 35 & 84 & 37.6 & 84.1 & 0 \\ 0 & 24.1 & 59.6 & 35 & 84.1 & 37.6 \\ 0 & 0 & 0 & 24.1 & 53.6 & 35 \\ 0 & 0 & 0 & 0 & 0 & 24.1 \end{bmatrix}$	$\begin{bmatrix} 34.1 & 1 & 0 & 0 & 0 & 0 \\ 0 & 37.4 & 34.1 & 1 & 310 & 0 \\ 0 & 0 & 52.3 & 37.6 & 84.1 & 0 \\ 0 & 0 & 0 & 12.2 & 33.1 & 37.6 \\ 0 & 0 & 0 & 0 & 11.8 & 39.3 \\ 0 & 0 & 0 & 0 & 0 & 24.1 \end{bmatrix}$	Hurwitz stable
$\mathcal{K}^2(s)$	$\begin{bmatrix} 50.9 & 1 & 0 & 0 & 0 & 0 \\ 84.1 & 56.2 & 50.9 & 1 & 0 & 0 \\ 80.1 & 35 & 84.1 & 56.2 & 50.9 & 0 \\ 0 & 35.9 & 80 & 35 & 84.1 & 56.2 \\ 0 & 0 & 0 & 35.9 & 80 & 35 \\ 0 & 0 & 0 & 0 & 0 & 35.9 \end{bmatrix}$	$\begin{bmatrix} 50.9 & 1 & 0 & 0 & 0 & 0 \\ 0 & 56.1 & 51.2 & 1 & 0 & 0 \\ 0 & 0 & 52.4 & 56.2 & 55.3 & 0 \\ 0 & 0 & 0 & 15.8 & 38.5 & 56.2 \\ 0 & 0 & 0 & 0 & 16.7 & 16.3 \\ 0 & 0 & 0 & 0 & 0 & 36.5 \end{bmatrix}$	Hurwitz stable
$\mathcal{K}^3(s)$	$\begin{bmatrix} 41.7 & 1 & 0 & 0 & 0 & 0 \\ 99.5 & 56.3 & 41.7 & 1 & 0 & 0 \\ 65.5 & 35.1 & 99.5 & 56.3 & 41.7 & 0 \\ 0 & 65.5 & 35.1 & 99.5 & 56.3 & 41.7 \\ 0 & 0 & 0 & 65.5 & 35.1 & 99.5 \\ 0 & 0 & 0 & 0 & 0 & 65.5 \end{bmatrix}$	$\begin{bmatrix} 41.7 & 1 & 0 & 0 & 0 & 0 \\ 0 & 52.3 & 41.7 & 1 & 0 & 0 \\ 0 & 0 & 76.8 & 56.2 & 41.7 & 0 \\ 0 & 0 & 0 & 101.2 & 63.7 & 41.7 \\ 0 & 0 & 0 & 0 & 20.3 & 78.5 \\ 0 & 0 & 0 & 0 & 0 & 65.5 \end{bmatrix}$	Hurwitz stable
$\mathcal{K}^4(s)$	$\begin{bmatrix} 41.7 & 1 & 0 & 0 & 0 & 0 \\ 68.9 & 37.7 & 41.8 & 1 & 0 & 0 \\ 37.2 & 35 & 68.9 & 37.7 & 41.8 & 0 \\ 0 & 24.1 & 37.2 & 35 & 68.9 & 37.7 \\ 0 & 0 & 0 & 24.1 & 37.2 & 35 \\ 0 & 0 & 0 & 0 & 0 & 24.1 \end{bmatrix}$	$\begin{bmatrix} 41.7 & 1 & 0 & 0 & 0 & 0 \\ 0 & 37.5 & 41.7 & 1 & 0 & 0 \\ 0 & 0 & 30.2 & 37.6 & 41.8 & 0 \\ 0 & 0 & 0 & 24.6 & 57.2 & 37.8 \\ 0 & 0 & 0 & 0 & 21.5 & 18.6 \\ 0 & 0 & 0 & 0 & 0 & 25.5 \end{bmatrix}$	Hurwitz stable

TABLE 6. Hurwitz matrix and row reduced Hurwitz matrix - CCTS.

Polynomial	HM	HM_n	Comments
$\mathcal{K}^1(s)$	$\begin{bmatrix} 44.3 & 1 & 0 & 0 & 0 & 0 \\ 30.9 & 71.7 & 44.3 & 1 & 0 & 0 \\ 47.8 & 31.1 & 30.8 & 71.7 & 44.3 & 0 \\ 0 & 19.2 & 47.8 & 31.1 & 30.8 & 71.7 \\ 0 & 0 & 0 & 19.2 & 47.8 & 31.1 \\ 0 & 0 & 0 & 0 & 0 & 19.2 \end{bmatrix}$	$\begin{bmatrix} 44.3 & 1 & 0 & 0 & 0 & 0 \\ 0 & 0.08 & 44.3 & 1 & 310 & 0 \\ 0 & 0 & 11.5 & 71.4 & 44.3 & 0 \\ 0 & 0 & 0 & 88.7 & 17.1 & 71.7 \\ 0 & 0 & 0 & 0 & 108 & 15.5 \\ 0 & 0 & 0 & 0 & 0 & 19.3 \end{bmatrix}$	Hurwitz stable
$\mathcal{K}^2(s)$	$\begin{bmatrix} 55.5 & 1 & 0 & 0 & 0 & 0 \\ 30.8 & 10.7 & 55.2 & 1 & 0 & 0 \\ 71.5 & 31.1 & 30.8 & 10.7 & 55.2 & 0 \\ 0 & 28.8 & 71.5 & 31.1 & 30.8 & 10.7 \\ 0 & 0 & 0 & 28.8 & 71.5 & 31.1 \\ 0 & 0 & 0 & 0 & 0 & 28.8 \end{bmatrix}$	$\begin{bmatrix} 55.5 & 11 & 0 & 0 & 0 & 0 \\ 0 & 47.1 & 55.3 & 1 & 0 & 0 \\ 0 & 0 & 11.5 & 10.7 & 55.3 & 0 \\ 0 & 0 & 0 & 65 & 11.4 & 10.72 \\ 0 & 0 & 0 & 0 & 12.2 & 78.5 \\ 0 & 0 & 0 & 0 & 0 & 28.7 \end{bmatrix}$	Hurwitz stable
$\mathcal{K}^3(s)$	$\begin{bmatrix} 54.1 & 1 & 0 & 0 & 0 & 0 \\ 37.8 & 10.8 & 54.2 & 1 & 0 & 0 \\ 58.4 & 31.1 & 37.8 & 10.8 & 54.2 & 0 \\ 0 & 28.8 & 58.4 & 31.1 & 37.8 & 10.8 \\ 0 & 0 & 0 & 28.8 & 58.4 & 31.1 \\ 0 & 0 & 0 & 0 & 0 & 28.8 \end{bmatrix}$	$\begin{bmatrix} 84.2 & 1 & 0 & 0 & 0 & 0 \\ 0 & 10.8 & 54.2 & 0 & 0 & 0 \\ 0 & 0 & 22.5 & 10.5 & 54.1 & 0 \\ 0 & 0 & 0 & 9.7 & 26.8 & 10.7 \\ 0 & 0 & 0 & 0 & 21.1 & 62.4 \\ 0 & 0 & 0 & 0 & 0 & 28.7 \end{bmatrix}$	Hurwitz stable
$\mathcal{K}^4(s)$	$\begin{bmatrix} 4.2 & 1 & 0 & 0 & 0 & 0 \\ 25.2 & 71.7 & 45.2 & 1 & 0 & 0 \\ 58.4 & 31.1 & 25.2 & 71.7 & 45.2 & 0 \\ 0 & 19.3 & 58.4 & 31.1 & 25.2 & 71.7 \\ 0 & 0 & 0 & 19.3 & 58.4 & 31.1 \\ 0 & 0 & 0 & 0 & 0 & 19.3 \end{bmatrix}$	$\begin{bmatrix} 45.2 & 1 & 0 & 0 & 0 & 0 \\ 0 & 71.1 & 45.2 & 1 & 0 & 0 \\ 0 & 0 & 55.5 & 71.3 & 45.2 & 0 \\ 0 & 0 & 0 & 28.2 & 12.3 & 71.7 \\ 0 & 0 & 0 & 0 & 50.1 & 36.2 \\ 0 & 0 & 0 & 0 & 0 & 19.3 \end{bmatrix}$	Hurwitz stable

COUPLED SPHERICAL TANK SYSTEM

Similarly, Table 5 presents the Hurwitz matrix and the row-reduced Hurwitz matrix for the Kharitonov polynomials for the CSTS. The proposed controller is robust stable as the diagonal elements are positive.

COUPLED CONICAL TANK SYSTEM

Subsequently, the Hurwitz matrix and the row-reduced Hurwitz matrix for the Kharitonov polynomials for the CCTS are presented in Table 6. The proposed controller is robust stable as the diagonal elements are positive.

STATEMENTS AND DECLARATIONS

COMPETING INTEREST

The authors have no relevant financial or non-financial interests to disclose.

AUTHORS CONTRIBUTIONS

The authors contributed equally to this work.

REFERENCES

[1] D. Shneiderman and Z. J. Palmor, "Properties and control of the quadruple-tank process with multivariable dead-times," *J. Process Control*, vol. 20, no. 1, pp. 18–28, Jan. 2010.

[2] E. Mirakhorli and M. Farrokhi, "Sliding-mode state-feedback control of non-minimum phase quadruple tank system using fuzzy logic," *IFAC Proc. Volumes*, vol. 44, no. 1, pp. 13546–13551, Jan. 2011.

[3] S. Sutha, P. Lakshmi, and S. Sankaranarayanan, "Fractional-order sliding mode controller design for a modified quadruple tank process via multi-level switching," *Comput. Electr. Eng.*, vol. 45, pp. 10–21, Jul. 2015.

[4] M. A. Nacusse and S. J. Junco, "Bond-graph-based controller design for the quadruple-tank process," *Int. J. Simul. Process Model.*, vol. 10, no. 2, pp. 179–191, 2015.

[5] C. Rajhans and S. Gupta, "Practical implementable controller design with guaranteed asymptotic stability for nonlinear systems," *Comput. Chem. Eng.*, vol. 163, Jul. 2022, Art. no. 107827.

[6] G. M. Tamilselvan and P. Aarthy, "Online tuning of fuzzy logic controller using Kalman algorithm for conical tank system," *J. Appl. Res. Technol.*, vol. 15, no. 5, pp. 492–503, Oct. 2017.

[7] T. Torres, J. Carlos, M. D. Mermoud, and O. Beytia, "Combining fractional order operators and adaptive passivity-based controllers: An application to the level regulation of a conical tank," *Romanian Soc. Control Eng. Tech. Informat.*, vol. 19, pp. 3–10, 2017.

[8] P. Ramanathan, K. K. Mangla, and S. Satpathy, "Smart controller for conical tank system using reinforcement learning algorithm," *Measurement*, vol. 116, pp. 422–428, Feb. 2018.

[9] R. Rajesh, "Optimal tuning of FOPID controller based on PSO algorithm with reference model for a single conical tank system, *Social Netw. Appl. Sci.*, vol. 1, no. 7, pp. 1–14, 2019.

[10] H. R. Patel and V. A. Shah, "Stable fault tolerant controller design for Takagi–Sugeno fuzzy model-based control systems via linear matrix inequalities: Three conical tank case study," *Energies*, vol. 12, no. 11, p. 2221, Jun. 2019.

[11] K. A. Sundari and P. Maruthupandi, "Optimal design of PID controller for the analysis of two TANK system using metaheuristic optimization algorithm," *J. Electr. Eng. Technol.*, vol. 17, no. 1, pp. 627–640, Jan. 2022.

[12] C. Sreepradha, P. Deepa, R. C. Panda, M. Manamali, and R. Shivakumar, "Synthesis of fuzzy sliding mode controller for liquid level control in spherical tank," *Cogent Eng.*, vol. 3, no. 1, Dec. 2016, Art. no. 1222042.

[13] M. Lakshmanan, K. Chitra, V. K. Kannan, and S. Srinivasan, "Online tuning of PI controller for spherical tank system using root locus technique with regulatory operation," in *Proc. 2nd Int. Conf. Inventive Res. Comput. Appl. (ICIRCA)*, Jul. 2020, pp. 1035–1041.

[14] G. M. Prasad and A. S. Rao, "Evaluation of gap-metric based multi-model control schemes for nonlinear systems: An experimental study," *ISA Trans.*, vol. 94, pp. 246–254, Nov. 2019.

[15] G. M. Prasad, A. Adithya, and A. S. Rao, "Design of multi model fractional controllers for nonlinear systems: An experimental investigation," *Comput. Aided Chem. Eng.*, vol. 46, pp. 1423–1428, 2019.

[16] C. Priya and P. Lakshmi, "Particle swarm optimisation applied to real time control of spherical tank system," *Int. J. Bio-Inspired Comput.*, vol. 4, no. 4, pp. 206–216, 2012.

[17] D. Soni, M. Gagrani, A. Rathore, and M. K. Chakravarthi, "Study of different controller's performance for a real time non-linear system," *Int. J. Adv. Electron. Electr. Eng.*, vol. 3, no. 3, pp. 1–5, 2014.

[18] K. V. Reshma and S. Sumathi, "Modelling and simulation of non linear spherical tank level process," *Asian J. Res. Social Sci. Hum.*, vol. 6, no. 5, pp. 18–40, 2016.

[19] D. Pradeepkannan and S. Sathiyamoorthy, "Control of a non-linear coupled spherical tank process using GA tuned PID controller," in *Proc. IEEE Int. Conf. Adv. Commun., Control Comput. Technol.*, May 2014, pp. 130–135.

[20] V. Kirubakaran, T. K. Radhakrishnan, and N. Sivakumaran, "Distributed multiparametric model predictive control design for a quadruple tank process," *Measurement*, vol. 47, pp. 841–854, Jan. 2014.

[21] C. M. Ionescu, A. Maxim, C. Copot, and R. De Keyser, "Robust PID auto-tuning for the quadruple tank system," *IFAC-PapersOnLine*, vol. 49, no. 7, pp. 919–924, 2016.

[22] D. H. Shah and D. M. Patel, "Design of sliding mode control for quadruple-tank MIMO process with time delay compensation," *J. Process Control*, vol. 76, pp. 46–61, Apr. 2019.

[23] B. Gurjar, V. Chaudhari, and S. Kurode, "Parameter estimation based robust liquid level control of quadruple tank system—Second order sliding mode approach," *J. Process Control*, vol. 104, pp. 1–10, Aug. 2021.

[24] X. Meng, H. Yu, J. Zhang, T. Xu, H. Wu, and K. Yan, "Disturbance observer-based feedback linearization control for a quadruple-tank liquid level system," *ISA Trans.*, vol. 122, pp. 146–162, Mar. 2022.

[25] V. R. Ravi and T. Thyagarajan, "Adaptive decentralized PI controller for two conical tank interacting level system," *Arabian J. Sci. Eng.*, vol. 39, no. 12, pp. 8433–8451, Dec. 2014.

[26] V. R. Ravi, T. Thyagarajan, and G. U. Maheshwaran, "Dynamic matrix control of a two conical tank interacting level system," *Proc. Eng.*, vol. 38, pp. 2601–2610, Jan. 2012.

[27] S. K. Lakshmanaprabu, M. Elhoseny, and K. Shankar, "Optimal tuning of decentralized fractional order PID controllers for TITO process using equivalent transfer function," *Cogn. Syst. Res.*, vol. 58, pp. 292–303, Dec. 2019.

[28] H. R. Patel and V. A. Shah, "A metaheuristic approach for interval type-2 fuzzy fractional order fault-tolerant controller for a class of uncertain nonlinear system*," *Automatika*, vol. 63, no. 4, pp. 656–675, Dec. 2022.

[29] M. K. Chakravarthi, V. K. Pannem, and N. Venkatesan, "Real time implementation of gain scheduled controller design for higher order non-linear system using LabVIEW," *Int. J. Eng. Technol.*, vol. 6, no. 5, pp. 2031–2038, 2014.

[30] A. Jegatheesh and C. A. Kumar, "Novel fuzzy fractional order PID controller for non linear interacting coupled spherical tank system for level process," *Microprocessors Microsyst.*, vol. 72, Feb. 2020, Art. no. 102948.

[31] A. V. Balakrishnaa and N. K. Arun, "Liquid level control of interacting coupled spherical tank system using PI and fuzzy PI controller," in *Proc. 3rd Int. Conf. Emerg. Technol. (INCET)*, May 2022, pp. 1–5.

[32] G. M. Prasad and A. S. Rao, "Multi-model cascade control strategy design based on gap metric for nonlinear processes," *Indian Chem. Eng.*, vol. 64, no. 2, pp. 183–196, Mar. 2022.

[33] K. R. A. Govind and S. Mahapatra, "Frequency domain specifications based robust decentralized PI/PID control algorithm for benchmark variable-area coupled tank systems," *Sensors*, vol. 22, no. 23, p. 9165, Nov. 2022.

[34] R. Mahadeva, M. Kumar, S. P. Patole, and G. Manik, "PID control design using AGPSO technique and its application in TITO reverse osmosis desalination plant," *IEEE Access*, vol. 10, pp. 125881–125892, 2022.

[35] J. Garrido, M. L. Ruz, F. Morilla, and F. Vázquez, "Iterative design of centralized PID controllers based on equivalent loop transfer functions and linear programming," *IEEE Access*, vol. 10, pp. 1440–1450, 2022.

[36] Y. Sun, J. Xu, G. Lin, and N. Sun, "Adaptive neural network control for maglev vehicle systems with time-varying mass and external disturbance," *Neural Comput. Appl.*, vol. 35, no. 17, pp. 12361–12372, Jun. 2023.

[37] J. Wang, Z. Deng, Z. Meng, and K. Shen, "Magnetoresistive sensor error compensation method using geometry-constraint contour scaling," *IEEE Trans. Instrum. Meas.*, vol. 71, pp. 1–9, 2022.

[38] R. Miranda-Colorado, "Closed-loop parameter identification of second-order non-linear systems: A distributional approach using delayed reference signals," *IET Control Theory Appl.*, vol. 13, no. 3, pp. 411–421, Feb. 2019.

[39] M. Lakshmanan, V. K. Kannan, K. Chitra, and S. Srinivasan, "Implementation of online self-tuning fuzzy-PI (STFPI) controller for conical tank system," in *Proc. ICIMES*. Hyderabad, India: Springer, 2020, pp. 185–194.

[40] P. Chandrasekar and L. Ponnusamy, "Research on variable area hybrid system using optimized fractional order control and passivity-based control," *Comput. Electr. Eng.*, vol. 57, pp. 324–335, Jan. 2017.

[41] L. Liu, S. Tian, D. Xue, T. Zhang, Y. Chen, and S. Zhang, "A review of industrial MIMO decoupling control," *Int. J. Control, Autom. Syst.*, vol. 17, no. 5, pp. 1246–1254, May 2019.

[42] K. R. A. Govind, S. Mahapatra, and S. R. Mahapatro, "A comparative analysis of various decoupling techniques using frequency domain specifications," in *Proc. 3rd Int. Conf. Artif. Intell. Signal Process. (AISP)*, Mar. 2023, pp. 1–6.

[43] S. K. Lakshmanaprabu and U. S. Banu, "Real time implementation of multivariable centralised FOPID controller for TITO process," *Int. J. Reasoning-Based Intell. Syst.*, vol. 10, no. 3, pp. 242–251, 2018.

[44] K. S. Ogunba, D. Fasiku, A. A. Fakunle, and O. Taiwo, "Analytical triangular decoupling internal model control of a class of two-input, two-output (TITO) systems with delays," *IFAC-PapersOnLine*, vol. 53, no. 2, pp. 4774–4779, 2020.

[45] S. K. Lakshmanaprabu, A. V. Nasir, and U. S. Banu, "Design of centralized fractional order PI controller for two interacting conical frustum tank level process," *J. Appl. Fluid Mech.*, vol. 10, pp. 23–32, Jan. 2017.

[46] S. K. Vavilala, V. Thirumavalavan, and K. Chandrasekaran, "Level control of a conical tank using the fractional order controller," *Comput. Electr. Eng.*, vol. 87, Oct. 2020, Art. no. 106690.

[47] D. Rosinová and A. Kozáková, "Decentralized robust control of MIMO systems: Quadruple tank case study," *IFAC Proc. Volumes*, vol. 45, no. 11, pp. 72–77, 2012.

[48] F. Garelli, R. J. Mantz, and H. De Battista, "Limiting interactions in decentralized control of MIMO systems," *J. Process Control*, vol. 16, no. 5, pp. 473–483, Jun. 2006.

[49] A. Osman, T. Kara, and M. Arıcı, "Robust adaptive control of a quadruple tank process with sliding mode and pole placement control strategies," *IETE J. Res.*, vol. 69, no. 5, pp. 2412–2425, 2023, doi: 10.1080/03772063.2021.1892537.

[50] W. Hu, G. Xiao, and X. Li, "An analytical method for PID controller tuning with specified gain and phase margins for integral plus time delay processes," *ISA Trans.*, vol. 50, no. 2, pp. 268–276, Apr. 2011.

[51] S. Skogestad and I. Postlethwaite, *Multivariable Feedback Control: Analysis and Design*, vol. 2. New York, NY, USA: Wiley, 2007.

[52] U. M. Nath, S. Datta, and C. Dey, "Centralized auto-tuned IMC-PI controllers for industrial coupled tank process with stability analysis," in *Proc. IEEE 2nd Int. Conf. Recent Trends Inf. Syst. (ReTIS)*, Jul. 2015, pp. 296–301.

[53] Y. V. Hote, "Necessary conditions for stability of Kharitonov polynomials," *IETE Tech. Rev.*, vol. 28, no. 5, pp. 445–448, 2011.

[54] K. R. A. Govind and S. Mahapatra, "Design of PI/PID control algorithm for a benchmark heat exchanger system using frequency domain specifications," in *Proc. IEEE Int. Power Renew. Energy Conf. (IPRECON)*, Dec. 2022, pp. 1–5.

[55] S. Mahapatra and K. R. A. Govind, "Design of a decentralised PI/PID control algorithm for a benchmark continuously stirred tank reactor system using frequency domain specifications," *Int. J. Model., Identificat. Control*, vol. 1, no. 1, p. 1, 2023, doi: 10.1504/IJMIC.2023.10054671.

[56] F. M. Hante, R. Krug, and M. Schmidt, "Time-domain decomposition for mixed-integer optimal control problems," *Appl. Math. Optim.*, vol. 87, no. 3, Jun. 2023.

[57] T. A. M. Euzébio, M. T. D. Silva, and A. S. Yamashita, "Decentralized PID controller tuning based on nonlinear optimization to minimize the disturbance effects in coupled loops," *IEEE Access*, vol. 9, pp. 156857–156867, 2021.

K. R. ACHU GOVIND received the B.Tech. degree from the Cochin University of Science and Technology, in 2012, and the M.Tech. degree from the University of Kerala, in 2014. He is currently pursuing the Ph.D. degree with the School of Electronics, VIT-AP University, Amaravathi, Andhra Pradesh. His research interests include control systems, nonlinear control, and biomedical instrumentation.

SUBHASISH MAHAPATRA (Senior Member, IEEE) received the master's degree majoring in instrumentation engineering from the Madras Institute of Technology Campus, Anna University, Chennai, in 2012, and the Ph.D. degree from the National Institute of Technology Rourkela, India, in 2018. Currently, he is a Senior Assistant Professor with the School of Electronics, Vellore Institute of Technology Andhra Pradesh, Amaravathi Campus, Andhra Pradesh, India. He was involved in various projects for organizations, such as DST and DRDO India towards the development of nonlinear control strategies for autonomous underwater vehicles. His research interests include the development of robust nonlinear control strategies for underwater robots, autonomous systems, and industrial systems.

SOUMYA RANJAN MAHAPATRO (Member, IEEE) received the M.Tech. and Ph.D. degrees in control system engineering from the National Institute of Technology Rourkela, India, in 2014 and 2018, respectively. He is currently an Associate Professor with the School of Electronics, Vellore Institute of Technology University, Chennai, Tamil Nadu, India. His research interests include process control, robust control and multivariable systems.